AGU ADVANCING EARTH AND SPACE SCIENCE

Geophysical Research Letters

RESEARCH LETTER
10.1029/2020GL090983

Special Section:
Atmospheric Rivers: Intersection of Weather and Climate

Atmospheric River Lifecycle Responses to the Madden-Julian Oscillation

Yang Zhou[1], Hyemi Kim[2], and Duane E. Waliser[3]

[1]Lawrence Berkeley National Laboratory, Berkeley, CA, USA, [2]Stony Brook University, Stony Brook, NY, USA, [3]Jet Propulsion Laboratory, California Institute of Technology, Pasadena, CA, USA

Abstract We investigate how the Madden-Julian Oscillation (MJO), the dominant mode of tropical subseasonal variability, modulates the lifecycle of cool-season North Pacific atmospheric rivers (ARs). When the enhanced (suppressed) convection center is located over the Indian Ocean (western Pacific), more AR events originate over eastern Asia and with fewer over the subtropical northern Pacific. When the enhanced (suppressed) convection is over the western Pacific (Indian Ocean), the opposite changes occur, with more AR events originate over the subtropical northern Pacific and fewer over eastern Asia. Dynamical processes involving anomalous MJO wind and seasonal mean moisture are found to be the dominant factors impacting these variations in AR origins. The MJO-related anomalous geopotential height patterns are also shown to modulate the propagation of the AR events. These MJO–AR lifecycle relationships are further supported by model simulations.

Plain Language Summary Atmospheric rivers (ARs) are strong moisture transport events that convey water vapor from the tropics to high latitudes. Precipitation generated from landfalling ARs is important freshwater sources to coastal regions like the west coast of North America. Here, we investigate the connections between the lifecycle of North Pacific ARs and the Madden-Julian Oscillation (MJO), which is the most dominant form of tropical subseasonal variability. Results indicate that the MJO can affect the whole lifecycle of ARs including the origin, propagation, and termination. ARs are more active during certain MJO phases, which can be explained by the changes in wind and geopotential height associated with the evolution and propagation of the MJO. These findings may help to better predict AR activity and understand how ARs will change in the future.

Key Points:

- The Madden-Julian Oscillation significantly influences the number, lifetime, and propagation of North Pacific atmospheric rivers (ARs)
- More ARs with longer lifetime occur over the subtropical North Pacific when enhanced convection is over the western Pacific
- Dynamical processes are the dominant factors in the modulation of ARs by the Madden-Julian Oscillation

Supporting Information:

- Supporting Information S1

Correspondence to:
Y. Zhou,
yzhou2@lbl.gov

Citation:
Zhou, Y., Kim, H., & Waliser, D. E. (2021). Atmospheric river lifecycle responses to the Madden-Julian Oscillation. *Geophysical Research Letters*, *48*, e2020GL090983. https://doi.org/10.1029/2020GL090983

Received 25 SEP 2020
Accepted 19 DEC 2020

1. Introduction

In the past 2 decades, atmospheric rivers (ARs) have garnered continuous scientific interest and public attention due to their contributions to regional hydrological impacts including sources of freshwater supply, snow accumulation, floods, and precipitation extremes (Dettinger, 2013; Gorodetskaya et al., 2014; Guan et al., 2010, 2013; Kamae et al., 2017; Lavers et al., 2011; Nash et al., 2018; Neiman et al., 2013; Waliser & Guan, 2017). While ARs are closely associated with midlatitude synoptic systems (J. W. Bao et al., 2006; Dacre et al., 2015; Z. Zhang et al., 2019), their activity is significantly modulated by modes of tropical variability like the Madden-Julian Oscillation (MJO, Guan & Waliser, 2015; Madden & Julian, 1972; Mundhenk et al., 2016; Payne & Magnusdottir, 2014), which has shown to have important impacts on midlatitude weather and climates (Ferranti et al., 1989; Stan et al., 2017; C. D. Zhang, 2013) such as storm tracks (Deng & Jiang, 2011; Zheng et al., 2018), atmospheric blocking events (Hamill & Kiladis, 2014; Henderson et al., 2016), and the Pacific-North America circulation pattern (Mori & Watanabe, 2008; J. Wang et al., 2020; W. Zhou et al., 2020). The landfalling ARs over North America and the associated California precipitation and snow accumulation are significantly intensified when the MJO convection is over the western Pacific (Guan et al., 2012, 2013; Payne & Magnusdottir, 2014). Given that the MJO is the dominant source of subseasonal predictability (Brunet et al., 2010; H. Kim et al., 2018; C. D. Zhang, 2013), the prediction of landfalling ARs shows some promise to be extended to 3–5 weeks lead time considering the MJO-AR connections (Baggett et al., 2017; DeFlorio et al., 2018, 2019; Mundhenk et al., 2018).

An AR event generally originates in the ocean and terminates after landfall (Guan & Waliser, 2019; Xu et al., 2020; Y. Zhou et al., 2018). The lifecycle of ARs, that is, the spatiotemporal evolution of moisture transport, is modulated by atmospheric circulation patterns (Guirguis et al., 2018; Y. Zhou & Kim, 2019).

However, it has to be established through what physical processes the MJO modulates the lifecycle of ARs from their origins to their terminations. So far, the MJO's impact on an AR lifecycle has only been discussed for a single landfalling AR event that occurred in March 2005 (Ralph et al., 2011). A better understanding of the MJO-AR lifecycle relationship can further help to improve the prediction of AR events and associated hydrological impacts. The goal of this study is to explore the physical mechanisms associated with the changes in AR lifecycles (origin, propagation, and termination) and their characteristics (number, lifetime, and intensity) that are affected by the MJO. The strong coupling between tropical moisture and convection is one of the key processes that explain the MJO dynamics (Adames & Kim, 2016; Bretherton et al., 2004; Holloway & Neelin, 2009; H. Kim et al., 2019) which distinguishes the MJO from other equatorial waves (Yasunaga & Mapes, 2012). The relative contributions to ARs from the changes in moisture versus wind that are associated with the MJO will be quantified and discussed in this study. The MJO may also modulate AR lifecycles via the teleconnection patterns related to the MJO diabatic heating anomalies. These hypotheses are tested with long historical high-resolution reanalysis data and numerical model simulations.

2. Data and Methods

2.1. Data

To investigate ARs, we use vertically integrated water vapor transport (IVT), which is calculated as

$$\mathrm{IVT} = -\frac{1}{g}\int_{1000\,\mathrm{hPa}}^{300\,\mathrm{hPa}} q\vec{V}\,dp, \tag{1}$$

where g is the gravitational acceleration (m s^{-2}), p is pressure (hPa), q is specific humidity (kg kg^{-1}), and $\vec{V}$ is horizontal wind vector (m s^{-1}). To calculate IVT, 20 vertical levels (1,000–300 hPa) of 1.0° six-hourly horizontal winds and specific humidity from European Centre for Medium-Range Weather Forecasts (ECMWF) Interim Reanalysis (ERAI, Dee et al., 2011) are used. Daily values of vertically integrated specific humidity, that is, precipitable water (PW), with 1.0° spatial resolution are used to represent general characteristics of the moisture field. We use 850 hPa 1.0° daily geopotential height (Z850) from ERAI to analyze AR-related circulations. Daily interpolated outgoing longwave radiation (OLR; Liebmann & Smith, 1996), with 2.5° spatial resolution, is used to indicate the MJO convection. The daily anomalies are calculated by subtracting the respective daily climatology and applying a 20–100-day Lanczos filtering to extract the intraseasonal signal. The analysis period is from 1979 to 2018 and Northern Hemisphere winter (November–March) when both MJO and North Pacific ARs are the most active (Guan & Waliser, 2015; Mundhenk et al., 2016; Stan et al., 2017).

2.2. The Madden-Julian Oscillation

The real-time multivariate MJO (RMM, Wheeler & Hendon, 2004) index is used to describe the MJO phase and amplitude. The RMM index consists of two principal components of a covariance matrix constructed by combined daily anomalies of OLR and zonal winds at 850 and 200 hPa in the tropics. The MJO is categorized into eight phases using two RMM components. In this study, an MJO day is defined if the RMM amplitude $\left(\sqrt{\mathrm{RMM1}^2 + \mathrm{RMM2}^2}\right)$ exceeds 1.0.

2.3. Lifecycle of ARs

To identify the lifecycle of AR events, we first detect the AR object which is defined as an enclosed 2-dimensional (latitude and longitude) instantaneous area of strong IVT that exceeds certain criteria of AR conditions (such as IVT magnitude and geometric constraints on length and width; Figure 1a). We follow the detection method developed by Guan and Waliser (2015) with minor modifications (i.e., reducing the IVT threshold to include more AR objects). The AR lifecycle is defined as a group of spatiotemporally connected AR objects, with the first object of the lifecycle defined as an AR origin (Y. Zhou et al., 2018). An

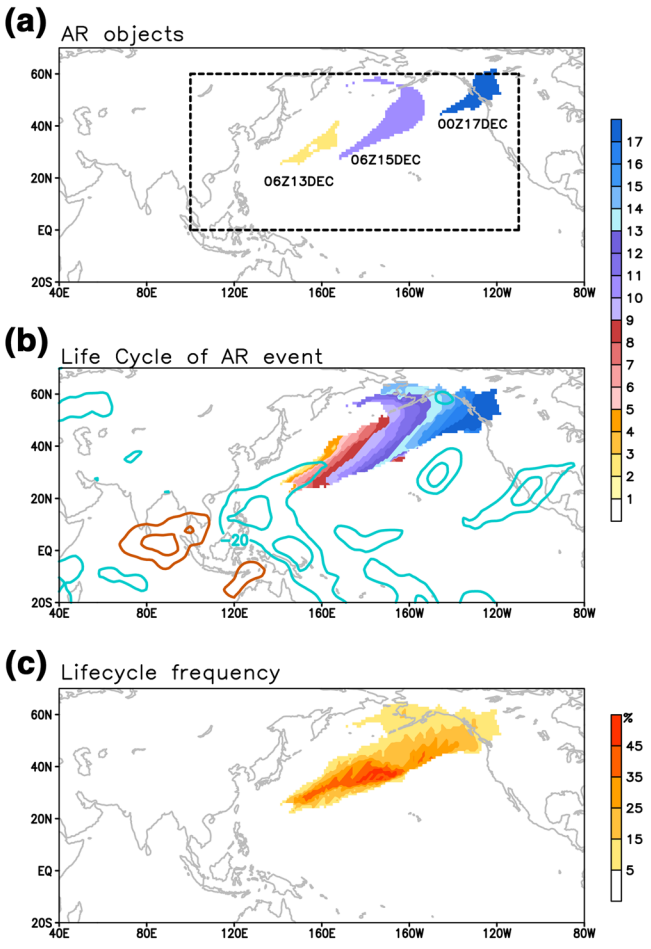

Figure 1. Example of (a) AR objects, (b) lifecycle, and (c) lifecycle frequency (percentage of objects during the lifetime of [b]) of a landfalling AR event during December 13–17, 2017. Dash box (0°N–60°N, 100°E–110°W) in (a) shows the focused region for AR lifecycles in this study. Shadings in (a) and (b) represent the binary masks of AR objects in 6-hourly time steps starting from the origin (December 13 00z). Orange/blue contours in (b) are 20–100-day-filtered OLR anomaly for positive/negative values (20 W m^{-2} interval, zero is omitted). AR, atmospheric river; OLR, outgoing longwave radiation.

example of an AR lifecycle that was concurrent with an MJO in phase 6 during December 13–17, 2017 is shown in Figure 1b. Associated lifecycle characteristics are shown that include AR lifetime, which shows how long an AR event lasts, and lifecycle intensity that represents the mean IVT magnitude during the lifecycle. The lifecycle frequency is calculated as the grid-point-accumulated number of AR objects (Figure 1b) from one lifecycle (Figure 1c) divided by the number of time steps. Hence, the lifecycle frequency is a density distribution that indicates the local occurrence of AR conditions over the period. For instance, within the lifetime of the AR event in Figure 1b (17 six-hourly time steps), some grid points over the central North Pacific are impacted by this AR for 45% of the lifetime (about 7–9 time steps), and grid points over the west coast of North America exhibit AR conditions for 5%–10% of the total AR lifetime (1–2 time steps; Figure 1c). The winter climatology of lifecycle frequency is computed by accumulating AR objects from all AR events and dividing it by the total number of six-hourly time steps during 39 winters (Figure 2a).

We categorize the AR events that originate between 0°N–60°N and 100°E–110°W (dash box in Figure 1a) by MJO phases. The changes in AR events are not sensitive to the domain boundary. For each MJO phase, an AR event is selected based on whether its origin is concurrent with that MJO phase (e.g., Figure 1b). Overall, approximately 63% of the total North Pacific AR events are selected. The composites of lifecycle frequency are constructed as follows: (i) for each MJO phase, select North Pacific AR events that *originate* concurrently with the MJO and (ii) compute the lifecycle frequency composite with the selected AR events and subtract the winter climatology (Figure 2a).

To make the results more concise and to increase sample sizes, we reduce the eight MJO phases into four groups (phases 8–1, 2–3, 4–5, and 6–7; e.g., Jeong et al., 2008; Li et al., 2016) and focus on MJO phases 2–3 and 6–7 when the most significant changes in lifecycle frequency are shown (Figure S1). Phase 2–3 exhibits enhanced (suppressed) convection over the Indian Ocean/western Pacific. Phase 6–7 is almost the opposite of phase 2–3. Figures 2b and 2c show the percentage changes in lifecycle frequency during phases 2–3 and 6–7 relative to the winter climatology.

2.4. Moisture Budget Decomposition

Previous studies have demonstrated that tropical intraseasonal variability like the MJO can modulate synoptic-scale disturbances via background flow or barotropic dynamics (e.g., Hsu et al., 2011; Kiladis et al., 2009; J. H. Kim et al., 2008; Sobel & Maloney, 2000; L. Wang & Wang, 2019; C. D. Zhang, 2005). We conduct moisture budget analysis on the anomalous moisture flux convergence (MFC). Similar to previous studies (H. Kim et al., 2017; Newman et al., 2012), we first decompose the total daily MFC field into climatological mean, anomalies, and nonlinear interactions between different time scales. Then, we only focus on the portion that is associated with the MJO (20–100-day filtered), which is represented by

$$\left(\mathrm{MFC}\right)' = \left(-\nabla\cdot\langle\overline{q}V'\rangle\right) + \left(-\nabla\cdot\langle q'\overline{V}\rangle\right) + \left(-\nabla\cdot\langle\left(q'V'\right)'\rangle\right), \tag{2}$$

where angled brackets represent vertical integration, overhead bars mark the seasonal mean, and prime signs mark the 20–100-day-filtered daily anomalies. The left-hand side represents the total anomalous MFC associated with the MJO. The terms on the right-hand side indicate the contributions from dynamic,

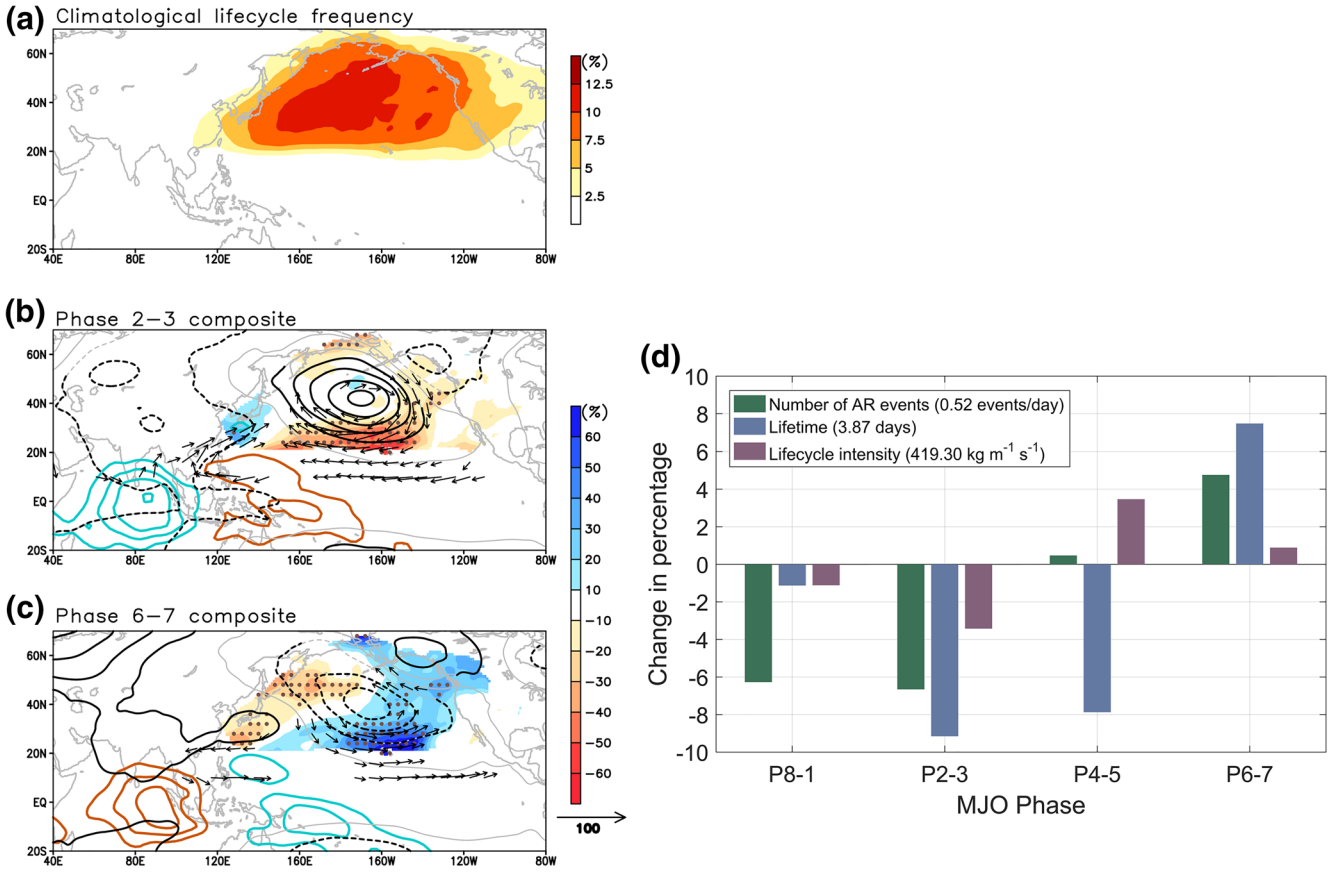

Figure 2. (a) Winter climatological lifecycle frequency (percent of time steps) with North Pacific AR events (originated in the black dash box in Figure 1a). (b, c) Percentage changes in lifecycle frequency relative to (a) (shading), Z850 anomaly (solid/dash contours represent positive/negative values, 5 m interval), IVT anomaly (vectors, only showing values to the north of 10°N and over 15 kg m $^{-1}$ s^{-1}), and OLR anomaly (orange/blue contours represent positive/negative values, 5 W/m^2 interval, zero line is omitted) for the MJO (b) phase 2–3 and (c) phase 6–7. Z850 and IVT anomalies are 10-day averaged starting from AR origins. The OLR anomaly is concurrent with AR origins. Dots mark AR frequency anomalies with $p < 0.05$ in one-sample t test. Black contours and vectors represent values with $p < 0.05$ in one-sample t test. (d) Percentage changes in the number of AR events, lifetime, and lifecycle intensity over the North Pacific. Numbers in the legend denote the climatological mean. AR, atmospheric river; IVT, integrated water vapor transport; OLR, outgoing longwave radiation; MJO, Madden-Julian Oscillation.

thermodynamic, and nonlinear components, respectively. Composites of MJO-associated moisture budget terms are based on the MJO days that are concurrent with the AR origin.

2.5. ECMWF AMIP Simulations

The robustness of the MJO-AR lifecycle relationship is examined with ECMWF AMIP simulations (ECMWF-Hist) with 10 ensemble members (Davini et al., 2017) and six-hourly output. The initial conditions are extracted from ERAI using the 00Z of the first 10 days starting from January 1, 1979. The sea surface temperature (SST) is obtained from the daily SST and sea ice concentration from Hadley Center Sea Ice and SST data set. The AMIP experiment extends from 1979 to 2008, and we analyze 20 winters (1980–2000). The model's horizontal resolution is T255 (~80 km) and is bilinearly interpolated to 1.0° to match with observations. The model's RMM index is obtained by projecting the model's OLR and 850 and 200 hPa zonal winds onto the observed eigenvectors from Wheeler and Hendon (2004). We preprocess the OLR and zonal winds by bilinearly interpolating them to 2.5° grid, removing the mean of the most recent 120 days of model analysis, and dividing by the observed normalization factors (details in Gottschalck et al., [2010]). The AR object detection in ECMWF-Hist is the same as ERAI. We treat each ensemble member equally and the ensemble mean is the average of selected AR lifecycles from 10 ensembles. We calculate the signal-to-noise ratio by dividing the signal which is the external forcing (ensemble mean of anomalous AR frequency) by

the noise which is the atmospheric internal variability (1 standard deviation of anomalous AR frequency across 10 ensemble members).

3. MJO's Impacts on AR Lifecycles

North Pacific AR activity peaks during boreal winter (Guan & Waliser, 2015; Mundhenk et al., 2016). Climatologically, the maximum lifecycle frequency emerges between 25°N and 60°N over the central North Pacific, indicating that more than 10% of winter time steps over the region are affected by ARs (Figure 2a). During MJO phase 2–3 (Figure 2b), a zonally oriented high-pressure anomaly prevails over the North Pacific and induces anomalous anticyclonic flow. Over eastern Asia, including the east coast of China, South Korea, and Japan, AR lifecycle frequency is increased by 10%–20% relative to climatology, corresponding to the anomalous poleward IVT to the west of the anomalous high. Over the subtropical North Pacific, which is associated with the anticyclonic flow, the lifecycle frequency is significantly suppressed by 50%–60% compared to climatology. The changes in lifecycle frequency are linked to changes in the number of AR events, lifetime, and lifecycle intensity. Over the North Pacific, all three factors (i.e., number, lifetime, and lifecycle intensity) consistently decrease during phase 2–3 (Figure 2d). Overall, the number of North Pacific AR events decreases by 6.7% in comparison with climatology (Figure 2d) and exhibits a significantly shortened lifetime and a weakened intensity.

The changes in lifecycle frequency during phase 6–7 (Figure 2c) show nearly the opposite features from MJO phase 2–3. The lifecycle frequency is reduced by about 30% over the northwestern Pacific, which is associated with the equatorward and westward IVT anomaly at the west of the prevailing anomalous cyclonic flow over the North Pacific. The anomalous cyclonic flow enhances AR activity by 30%–60% over the central North Pacific and 20%–30% over northwestern North America relative to climatology. The AR activity near Hawaii, sometimes referred to as Pineapple Express events, is more frequent during MJO phase 6–7 which potentially leads to more AR landfalls over the west coast of North America (Guan et al., 2012; Payne & Magnusdottir, 2014; Spry et al., 2014). The number of AR events increases by nearly 5% during phase 6–7 with a significantly longer lifetime and stronger intensity (Figure 2d).

4. Physical Mechanism Behind the MJO-AR Lifecycle Relationship

The results indicate that the propagation of ARs during their lifecycles roughly aligns with the geopotential height anomalies (Figure S2). During MJO phase 2–3, an increased frequency of AR origins occurs over eastern Asia (Figures 3a and S2a). The increased frequency extends northward along the northwest flank of the anomalous high and gradually dissipates about 4 days after AR origins (Figure S2c), likely due to having less overall moisture content in the higher latitudes which expedites the termination of the AR events (Trenberth, 1998). Meanwhile, the decreased frequency associated with the anticyclonic flow persists over the subtropical Pacific until 6 days after the AR origins (Figure S2d). In contrast, during phase 6–7, increased (decreased) frequency of AR origins occurs over the subtropical northwestern Pacific (eastern Asia; Figures 3b and S2f). After the AR origins, the increased frequency amplifies as it extends eastward and northward for 6 days, accompanied by the anomalous low and cyclonic flow (Figures S2f–S2i).

The results discussed above show that the MJO influences the entire AR lifecycle including the origins. Through what physical processes does the MJO influence the origin of ARs? Studies have elucidated that the MJO-associated tropical heating induces the Matsuno-Gill response (M. Bao & Hartmann, 2014; Gill, 1980; Matsuno, 1966), and the enhanced tropical convection is strongly coupled to moisture (Bretherton et al., 2004). During MJO phase 2–3 (Figure 3a), higher PW is observed in the Indo-Pacific and East Asia. Two anticyclonic anomalies arise near 135°E on each side of the equator, which are to the west of the suppressed convection over the western Pacific, a typical Matsuno-Gill type response. The associated anomalous poleward wind near 30°N, 120°E advects the mean moisture (discussed below) and supports the increase of AR origins over eastern Asia. Meanwhile, the decreased frequency of AR origins near 160°E is associated with the southwestward IVT anomaly related to the decreased moisture and southward wind anomalies. Conversely, during MJO phase 6–7 (Figure 3b), Indo-Pacific and eastern Asia are drier overall and two cyclonic flow anomalies straddle the equator over the western Pacific. The decreased frequency of AR origins over eastern Asia is attributed to the decreased moisture and southwestward wind anomalies.

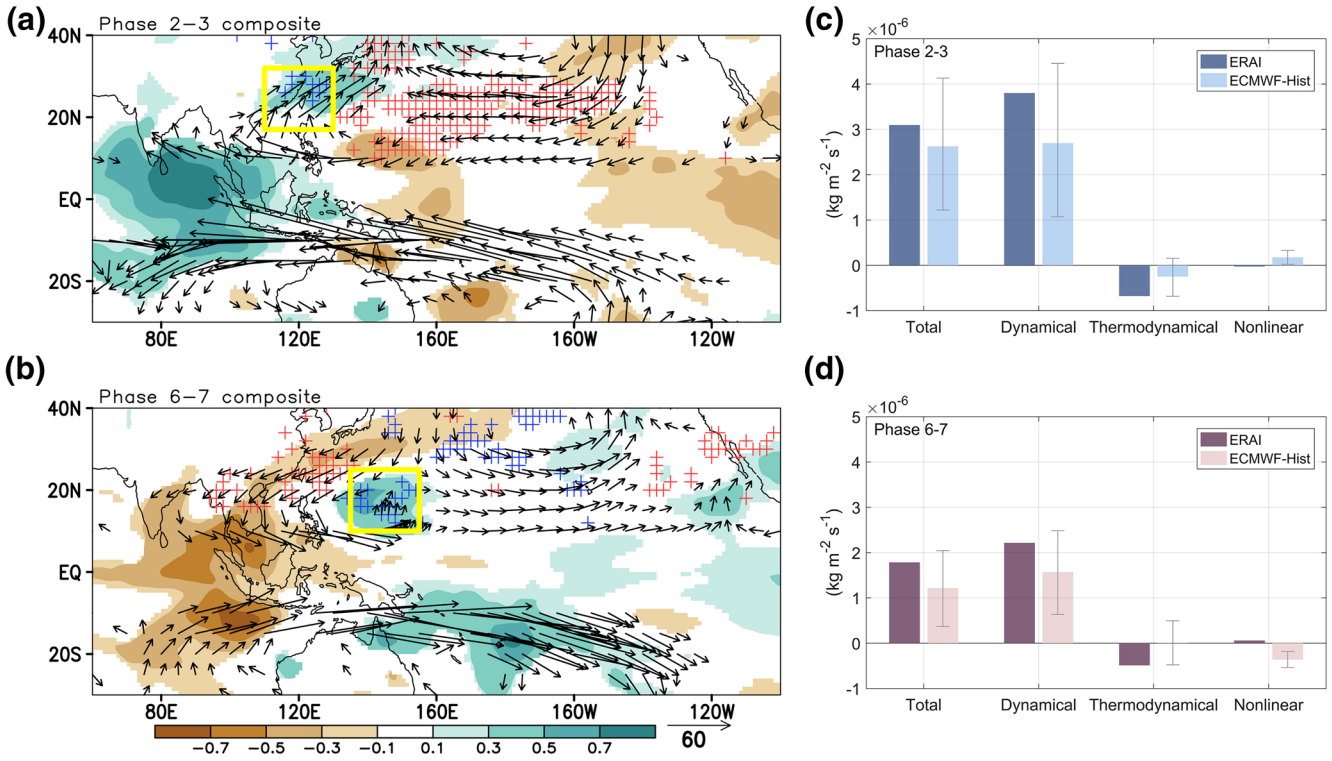

Figure 3. A 20–100-day-filtered precipitable water anomaly (shading, kg m^{-2}) and IVT anomaly (vectors, only showing values outside of 10°S–10°N and over 10 kg m^{-1} s^{-1}), and AR origin frequency anomaly (blue/red cross markers represent positive/negative values with $p < 0.1$ in one-sample t test) for the MJO (a) phase 2–3 and (b) phase 6–7. Vectors and shadings represent values with $p < 0.05$ in one-sample t test. (c, d) Moisture budget terms for the MJO (c) phase 2–3 and (d) phase 6–7 averaged within the yellow box (17°N–32°N, 110°E–130°E in [a] and 10°N–25°N, 135°E–155°E in [b]) using ERA-I and ECMWF-Hist. The bars in (c) and (d) show the ensemble means of ECMWF-Hist and the error bars show the 1 standard deviation of 10 ensemble members. ECMWF, European Centre for Medium-Range Weather Forecasts; IVT, integrated water vapor transport; AR, atmospheric river; MJO, Madden-Julian Oscillation.

The increased moisture and cyclonic flow anomalies facilitate the increased frequency of AR origins near 150°E. In addition, for both phases 2–3 and 6–7, changes in origin frequency over the subtropical central North Pacific are aligned with the southern flank of geopotential height anomaly and facilitated by the corresponding anomalous IVT (Figures 3a and 3b).

To better understand the relative contributions from dynamic (wind), thermodynamic (moisture), and nonlinear processes, we decompose the anomalous MFC that corresponds to areas of increased frequency of AR origins (yellow boxes in Figures 3a and 3b). The results indicate that the dynamical process related to seasonal mean moisture variations and anomalous MJO wind contributes the most to changes in total MFC in MJO phases 2–3 and 6–7 (Figures 3c and 3d). The thermodynamic process, which is associated with seasonal mean wind and the MJO moisture anomaly, contributes negatively to the total changes: although the moisture anomaly becomes positive as the MJO propagates, a positive meridional gradient in seasonal mean meridional wind leads to a decrease in local MFC. The nonlinear component associated with the MJO moisture and wind anomalies is negligible for both phases. Moreover, the amplitude difference in total MFC anomaly between MJO phases 2–3 and 6–7 is primarily due to the meridional gradient of mean moisture (Figure 4): over the subtropical northwestern Pacific (where AR origin is enhanced during phase 2–3), the meridional distribution of mean moisture is steeper than that over the tropics (where AR origin is enhanced during phase 6–7).

The extent to which the observed MJO-AR lifecycle relationship is affected by atmospheric internal variability is unclear. To expand sample sizes and to evaluate the robustness of the observed connection, the MJO-AR lifecycle relationship is examined in ECMWF AMIP simulations, which have shown improvement in simulating the MJO propagation (Davini et al., 2017). Overall, the simulated changes in lifecycle frequency are roughly consistent with the observation, albeit with weaker amplitude and regional biases (Figures S3a

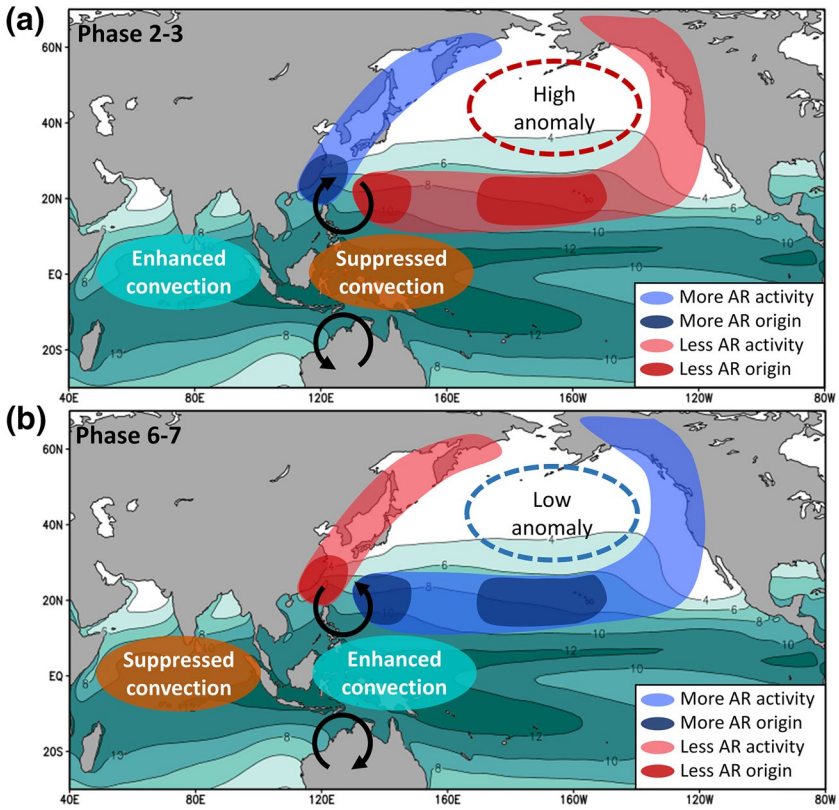

Figure 4. Schematic diagrams of the MJO's impact on AR lifecycles during the MJO (a) phase 2–3 and (b) phase 6–7. Background shading is 850 hPa specific humidity climatology (g/kg). Curved black arrows mark the anomalous 850 hPa wind as Matsuno-Gill response. MJO, Madden-Julian Oscillation; AR, atmospheric river.

and S3b). The model simulates the observed physical processes (Figures 3c and 3d), which indicates the dominant role of the MJO-related wind in the MJO-AR lifecycle connection. With the presence of internal variability (noise), changes in simulated AR activity over the North Pacific are largely controlled by the MJO (signal; Figures S3c and S3d).

5. Summary

We explore the physical processes of the MJO-AR lifecycle relationship over the North Pacific by tracking the lifecycle of ARs from their origins to their terminations. Figure 4 summarizes the key results. Changes in AR lifecycles are most significant during MJO phase 2–3 and 6–7 when a dipole of enhanced and suppressed convections locates over the Indian Ocean and the western Pacific. During MJO phase 2–3, an increased (decreased) frequency of AR origins occurs over eastern Asia (the northwestern Pacific), which is associated with the anticyclonic flows over the subtropical western Pacific. The propagation of ARs is influenced by the persistent high-pressure circulation anomaly, with decreased (increased) AR activity over the subtropical central Pacific (northwestern Pacific). The opposite features emerge during MJO phase 6–7: the anomalous low-pressure circulation prevails over the northern Pacific and guides ARs to propagate northeastward. AR activity is decreased northwest of the anomalous low. Responses in AR lifecycle are influenced most strongly by the combined MJO wind anomaly and seasonal mean moisture patterns. Model simulations further support the robustness of the relation of the MJO and AR lifecycles.

Since ARs are often synonymous with severe weather events, improving subseasonal prediction of ARs is of great importance to facilitate emergency preparedness and to mitigate socio-economic losses (Dominguez et al., 2018; Ralph et al., 2019). While previous studies mainly focus on the prediction of landfalling AR frequency related to the MJO (Baggett et al., 2017; DeFlorio et al., 2018, 2019; Mundhenk et al., 2018), the analyzed connection between the MJO and AR lifecycle may potentially help to improve the subseasonal

prediction of ARs utilizing the correspondence between AR origins and terminations (which are often associated with precipitation at landfall). For instance, with a given MJO phase or its forecasted state, one could possibly forecast the lifecycle of an AR event including its likely propagation track and termination location and further its hydrological impacts.

Finally, questions have been raised about how ARs will change in the future climate. AR occurrence is projected to increase (Dettinger, 2011; Lavers et al., 2013; Warner et al., 2015) with longer and wider geometric shapes, stronger intensities, and a poleward shift of landfall locations (Espinoza et al., 2018; Ma et al., 2020; Radic et al., 2015; Shields & Kiehl, 2016). The MJO is projected to have deeper and larger convection and to travel further eastward with increasing phase speed (Adames et al., 2017; Chang et al., 2015; Maloney et al., 2019). The projected circulation responses to the MJO show a large diversity among models (Bui & Maloney, 2018; Wolding et al., 2017; W. Zhou et al., 2020). Therefore, future changes of the MJO-AR connection deserve further investigation. The current study provides a scientific basis and useful perspective to examine the MJO-AR connection in the context of future climate.

Data Availability Statement

ERA-Interim data were obtained freely from http://apps.ecmwf.int/datasets/data/interim_full_daily. The OLR is provided by the NOAA/OAR/ESRL PSD, Boulder, CO, USA, from their Web site at https://psl.noaa.gov/data/gridded/data.interp_OLR.html. The RMM index is obtained from the Bureau of Meteorology from Australian Government (http://www.bom.gov.au/climate/mjo/graphics/rmm.74toRealtime.txt). The ECMWF AMIP simulation is provided by Dr. Aneesh Subramanian which can be downloaded through a dedicated THREDDS Web Server hosted by CINECA (https://sphinx.hpc.cineca.it/thredds/catalog/SPHINX/catalog.html).

Acknowledgments
The authors would like to acknowledge the two anonymous reviews for their constructive and thoughtful comments about our manuscript. Y. Zhou was supported by NSF grant AGS-1652289 and the U.S. Department of Energy, Office of Science, Office of Biological and Environmental Research, Climate and Environmental Sciences Division, Regional & Global Climate Modeling Program, under Award DE-AC02-05CH11231. H. Kim was supported by NSF grant AGS-1652289 and the KMA R&D Program grant KMI2018-03110. D.E.W.'s contribution to this study was carried out on behalf of the Jet Propulsion Laboratory, California Institute of Technology, under a contract with the National Aeronautics and Space Administration. The authors thank Dr. Aneesh Subramanian for sharing the ECMWF AMIP simulation data.

References

Adames, A. F., & Kim, D. (2016). The MJO as a dispersive, convectively coupled moisture wave: Theory and observations. *Journal of the Atmospheric Sciences*, *73*(3), 913–941. https://doi.org/10.1175/JAS-D-15-0170.1

Adames, A. F., Kim, D., Sobel, A. H., Del Genio, A., & Wu, J. (2017). Changes in the structure and propagation of the MJO with increasing CO_2. *Journal of Advances in Modeling Earth Systems*, *9*(2), 1251–1268. https://doi.org/10.1002/2017MS000913

Baggett, C. F., Barnes, E. A., Maloney, E. D., & Mundhenk, B. D. (2017). Advancing atmospheric river forecasts into subseasonal-to-seasonal time scales. *Geophysical Research Letters*, *44*(14), 7528–7536. https://doi.org/10.1002/2017GL074434

Bao, J. W., Michelson, S. A., Neiman, P. J., Ralph, F. M., & Wilczak, J. M. (2006). Interpretation of enhanced integrated water vapor bands associated with extratropical cyclones: Their formation and connection to tropical moisture. *Monthly Weather Review*, *134*(4), 1063–1080. https://doi.org/10.1175/MWR3123.1

Bao, M., & Hartmann, D. L. (2014). The response to MJO-like forcing in a nonlinear shallow-water model. *Geophysical Research Letters*, *41*(4), 1322–1328. https://doi.org/10.1002/2013GL057683

Bretherton, C. S., Peters, M. E., & Back, L. E. (2004). Relationships between water vapor path and precipitation over the tropical oceans. *Journal of Climate*, *17*(7), 1517–1528. https://doi.org/10.1175/1520-0442(2004)017<1517:RBWVPA>2.0.CO;2

Brunet, G., Shapiro, M., Hoskins, B., Moncrieff, M., Dole, R., Kiladis, G. N., et al. (2010). Collaboration of the weather and climate communities to advance subseasonal-to-seasonal prediction. *Bulletin of the American Meteorological Society*, *91*(10), 1397–1406. https://doi.org/10.1175/2010BAMS3013.1

Bui, H. X., & Maloney, E. D. (2018). Changes in Madden-Julian Oscillation precipitation and wind variance under global warming. *Geophysical Research Letters*, *45*(14), 7148–7155. https://doi.org/10.1029/2018GL078504

Chang, C. W. J. N., Tseng, W. L., Hsu, H. H., Keenlyside, N., & Tsuang, B. J. (2015). The Madden-Julian Oscillation in a warmer world. *Geophysical Research Letters*, *42*(14), 6034–6042. https://doi.org/10.1002/2015GL065095

Dacre, H. F., Clark, P. A., Martinez-Alvarado, O., Stringer, M. A., & Lavers, D. A. (2015). How do atmospheric rivers form? *Bulletin of the American Meteorological Society*, *96*(8), 1243–1255. https://doi.org/10.1175/BAMS-D-14-00031.1

Davini, P., von Hardenberg, J., Corti, S., Christensen, H. M., Juricke, S., Subramanian, A., et al. (2017). Climate SPHINX: Evaluating the impact of resolution and stochastic physics parameterisations in the EC-Earth global climate model. *Geoscientific Model Development*, *10*(3), 1383–1402. https://doi.org/10.5194/gmd-10-1383-2017

Dee, D. P., Uppala, S. M., Simmons, A. J., Berrisford, P., Poli, P., Kobayashi, S., et al. (2011). The ERA-Interim reanalysis: Configuration and performance of the data assimilation system. *Quarterly Journal of the Royal Meteorological Society*, *137*(656), 553–597. https://doi.org/10.1002/qj.828

DeFlorio, M. J., Waliser, D. E., Guan, B., Ralph, F. M., & Vitart, F. (2018). Global evaluation of atmospheric river subseasonal prediction skill. *Climate Dynamics*, *52*(5–6), 3039–3060. https://doi.org/10.1007/s00382-018-4309-x

DeFlorio, M. J., Waliser, D. E., Ralph, F. M., Guan, B., Goodman, A., Gibson, P. B., et al. (2019). Experimental subseasonal-to-seasonal (S2S) forecasting of atmospheric rivers over the Western United States. *Journal of Geophysical Research: Atmospheres*, *124*(21), 11242–11265. https://doi.org/10.1029/2019JD031200

Deng, Y., & Jiang, T. Y. (2011). Intraseasonal modulation of the North Pacific storm track by tropical convection in boreal winter. *Journal of Climate*, *24*(4), 1122–1137. https://doi.org/10.1175/2010JCLI3676.1

Dettinger, M. D. (2011). Climate change, atmospheric rivers, and floods in California—A multimodel analysis of storm frequency and magnitude changes. *Journal of the American Water Resources Association*, *47*(3), 514–523. https://doi.org/10.1111/j.1752-1688.2011.00546.x

Dettinger, M. D. (2013). Atmospheric rivers as drought busters on the US West Coast. *Journal of Hydrometeorology*, *14*(6), 1721–1732. https://doi.org/10.1175/JHM-D-13-02.1

Dominguez, F., Dall'erba, S., Huang, S., Avelino, A., Mehran, A., Hu, H., et al. (2018). Tracking an atmospheric river in a warmer climate: From water vapor to economic impacts. *Earth System Dynamics*, *9*(1), 249–266. https://doi.org/10.5194/esd-9-249-2018

Espinoza, V., Waliser, D. E., Guan, B., Lavers, D. A., & Ralph, F. M. (2018). Global analysis of climate change projection effects on atmospheric rivers. *Geophysical Research Letters*, *45*(9), 4299–4308. https://doi.org/10.1029/2017GL076968

Ferranti, L., Palmer, T. N., Molteni, F., & Klinker, E. (1989). Tropical–extratropical interaction associated with the 30–60 day oscillation and its impact on medium and extended range prediction. *Journal of the Atmospheric Sciences*, *47*(18), 2177–2199. https://doi.org/10.1175/1520-0469(1990)047<2177:TEIAWT>2.0.CO;2

Gill, A. E. (1980). Some simple solutions for heat-induced tropical circulation. *Quarterly Journal of the Royal Meteorological Society*, *106*(449), 447–462. https://doi.org/10.1002/qj.49710644905

Gorodetskaya, I. V., Tsukernik, M., Claes, K., Ralph, M. F., Neff, W. D., & Van Lipzig, N. P. M. (2014). The role of atmospheric rivers in anomalous snow accumulation in East Antarctica. *Geophysical Research Letters*, *41*(17), 6199–6206. https://doi.org/10.1002/2014GL060881

Gottschalck, J., Wheeler, M., Weickmann, K., Vitart, F., Savage, N., Lin, H., et al. (2010). A framework for assessing operational Madden-Julian Oscillation forecasts. *Bulletin of the American Meteorological Society*, *91*(9), 1247–1258. https://doi.org/10.1175/2010BAMS2816.1

Guan, B., Molotch, N. P., Waliser, D. E., Fetzer, E. J., & Neiman, P. J. (2010). Extreme snowfall events linked to atmospheric rivers and surface air temperature via satellite measurements. *Geophysical Research Letters*, *37*(20), L20401. https://doi.org/10.1029/2010GL044696

Guan, B., Molotch, N. P., Waliser, D. E., Fetzer, E. J., & Neiman, P. J. (2013). The 2010/2011 snow season in California's Sierra Nevada: Role of atmospheric rivers and modes of large-scale variability. *Water Resources Research*, *49*(10), 6731–6743. https://doi.org/10.1002/wrcr.20537

Guan, B., & Waliser, D. E. (2015). Detection of atmospheric rivers: Evaluation and application of an algorithm for global studies. *Journal of Geophysical Research: Atmospheres*, *120*(24), 12514–12535. https://doi.org/10.1002/2015JD024257

Guan, B., & Waliser, D. E. (2019). Tracking atmospheric rivers globally: Spatial distributions and temporal evolution of life cycle characteristics. *Journal of Geophysical Research: Atmospheres*, *124*(23), 12523–12552. https://doi.org/10.1029/2019JD031205

Guan, B., Waliser, D. E., Molotch, N. P., Fetzer, E. J., & Neiman, P. J. (2012). Does the Madden-Julian Oscillation influence wintertime atmospheric rivers and snowpack in the Sierra Nevada? *Monthly Weather Review*, *140*(2), 325–342. https://doi.org/10.1175/MWR-D-11-00087.1

Guirguis, K., Gershunov, A., Shulgina, T., Clemesha, R. E. S., & Ralph, F. M. (2018). Atmospheric rivers impacting Northern California and their modulation by a variable climate. *Climate Dynamics*, *52*(11), 6569–6583. https://doi.org/10.1007/s00382-018-4532-5

Hamill, T. M., & Kiladis, G. N. (2014). Skill of the MJO and Northern Hemisphere blocking in GEFS medium-range reforecasts. *Monthly Weather Review*, *142*(2), 868–885. https://doi.org/10.1175/MWR-D-13-00199.1

Henderson, S. A., Maloney, E. D., & Barnes, E. A. (2016). The influence of the Madden-Julian Oscillation on Northern Hemisphere winter blocking. *Journal of Climate*, *29*(12), 4597–4616. https://doi.org/10.1175/JCLI-D-15-0502.1

Holloway, C. E., & Neelin, J. D. (2009). Moisture vertical structure, column water vapor, and tropical deep convection. *Journal of the Atmospheric Sciences*, *66*(6), 1665–1683. https://doi.org/10.1175/2008JAS2806.1

Hsu, P., Li, T., & Tsou, C. (2011). Interactions between boreal summer intraseasonal oscillations and synoptic-scale disturbances over the Western North Pacific. Part I: Energetics diagnosis. *Journal of Climate*, *24*(3), 927–941. https://doi.org/10.1175/2010JCLI3833.1

Jeong, J., Kim, B., Ho, C., & Noh, Y. (2008). Systematic variation in wintertime precipitation in East Asia by MJO-induced extratropical vertical motion. *Journal of Climate*, *21*(4), 788–801. https://doi.org/10.1175/2007JCLI1801.1

Kamae, Y., Mei, W., Xie, S.-P., Naoi, M., & Ueda, H. (2017). Atmospheric rivers over the northwestern Pacific: Climatology and interannual variability. *Journal of Climate*, *30*(15), 5605–5619. https://doi.org/10.1175/JCLI-D-16-0875.1

Kiladis, G. N., Wheeler, M. C., Haertel, P. T., Straub, K. H., & Roundy, P. E. (2009). Convectively coupled equatorial waves. *Reviews of Geophysics*, *47*(2), 266–308. https://doi.org/10.1029/2008RG000266

Kim, H., Janiga, M. A., & Pegion, K. (2019). MJO propagation processes and mean biases in the SubX and S2S reforecasts. *Journal of Geophysical Research: Atmospheres*, *124*(16), 9314–9331. https://doi.org/10.1029/2019JD031139

Kim, H., Vitart, F., & Waliser, D. E. (2018). Prediction of the Madden-Julian Oscillation: A review. *Journal of Climate*, *31*(23), 9425–9443. https://doi.org/10.1175/JCLI-D-18-0210.1

Kim, H., Zhou, Y., & Alexander, M. A. (2017). Changes in atmospheric rivers and moisture transport over the Northeast Pacific and western North America in response to ENSO diversity. *Climate Dynamics*, *52*(5-6), 7375–7388. https://doi.org/10.1007/s00382-017-3598-9

Kim, J. H., Ho, C. H., Kim, H. S., Sui, C. H., & Park, S. K. (2008). Systematic variation of summertime tropical cyclone activity in the western North Pacific in relation to the Madden-Julian Oscillation, *Journal of Climate*, *21*(6), 1171–1191, https://doi.org/10.1175/2007JCLI1493.1

Lavers, D. A., Allan, R. P., Villarini, G., Lloyd-Hughes, B., Brayshaw, D. J., & Wade, A. J. (2013). Future changes in atmospheric rivers and their implications for winter flooding in Britain. *Environmental Research Letters*, *8*(3), 034010–034018. https://doi.org/10.1088/1748-9326/8/3/034010

Lavers, D. A., Allan, R. P., Wood, E. F., Villarini, G., Brayshaw, D. J., & Wade, A. J. (2011). Winter floods in Britain are connected to atmospheric rivers. *Geophysical Research Letters*, *38*(23), L23803. https://doi.org/10.1029/2011GL049783

Li, W., Guo, W., Hsu, P., & Xue, Y. (2016). Influence of the Madden-Julian Oscillation on Tibetan Plateau snow cover at the intraseasonal time-scale. *Scientific Reports*, *6*(1), 30456–30465. https://doi.org/10.1038/srep30456

Liebmann, B., & Smith, C. A. (1996). Description of a complete (interpolated) outgoing longwave radiation dataset. *Bulletin of the American Meteorological Society*, *77*(6), 1275–1277.Retrieved from <Go to ISI>://WOS:A1996VC04300013

Ma, W., Chen, G., & Guan, B. (2020). Poleward shift of atmospheric rivers in the Southern Hemisphere in recent decades. *Geophysical Research Letters*, *47*(21), e2020GL089934. https://doi.org/10.1029/2020GL089934

Madden, R., & Julian, P. (1972). Further evidence of global-scale, 5-day pressure waves. *Journal of the Atmospheric Sciences*, *29*(8), 1464–1469. https://doi.org/10.1175/1520-0469(1972)029<1464:FEOGSD>2.0.CO;2

Maloney, E. D., Adames, A. F., & Bui, H. X. (2019). Madden-Julian Oscillation changes under anthropogenic warming. *Nature Climate Change*, *9*(1), 26–33. https://doi.org/10.1038/s41558-018-0331-6

Matsuno, T. (1966). Quasi-geostrophic motions in the equatorial area. *Journal of the Meteorological Society of Japan. Series II*, *44*(1), 25–43. https://doi.org/10.2151/jmsj1965.44.1_25

Mori, M., & Watanabe, M. (2008). Growth and triggering mechanisms of the PNA: A MJO-PNA coherence. *Journal of the Meteorological Society of Japan*, *86*(1), 213–236. https://doi.org/10.2151/jmsj.86.213

Mundhenk, B. D., Barnes, E. A., & Maloney, E. D. (2016). All-season climatology and variability of atmospheric river frequencies over the North Pacific. *Journal of Climate*, *29*(13), 4885–4903. https://doi.org/10.1175/JCLI-D-15-0655.1

Mundhenk, B. D., Barnes, E. A., Maloney, E. D., & Baggett, C. F. (2018). Skillful empirical subseasonal prediction of landfalling atmospheric river activity using the Madden-Julian Oscillation and quasi-biennial oscillation. *npj Climate and Atmospheric Science*, *1*(1), 20177. https://doi.org/10.1038/s41612-017-0008-2

Nash, D., Waliser, D., Guan, B., Ye, H., & Ralph, F. M. (2018). The role of atmospheric rivers in extratropical and polar hydroclimate. *Journal of Geophysical Research: Atmospheres*, *123*(13), 6804–6821. https://doi.org/10.1029/2017JD028130

Neiman, P. J., Ralph, F. M., Moore, B. J., Hughes, M., Mahoney, K. M., Cordeira, J. M., & Dettinger, M. D. (2013). The landfall and inland penetration of a flood-producing atmospheric river in Arizona. Part I: Observed synoptic-scale, orographic, and hydrometeorological characteristics. *Journal of Hydrometeorology*, *14*(2), 460–484. https://doi.org/10.1175/JHM-D-12-0101.1

Newman, M., Kiladis, G. N., Weickmann, K. M., Ralph, F. M., & Sardeshmukh, P. D. (2012). Relative contributions of synoptic and low-frequency eddies to time-mean atmospheric moisture transport, including the role of atmospheric rivers. *Journal of Climate*, *25*(21), 7341–7361. https://doi.org/10.1175/JCLI-D-11-00665.1

Payne, A. E., & Magnusdottir, G. (2014). Dynamics of landfalling atmospheric rivers over the North Pacific in 30 years of MERRA reanalysis. *Journal of Climate*, *27*(18), 7133–7150. https://doi.org/10.1175/JCLI-D-14-00034.1

Radic, V., Cannon, A. J., Menounos, B., & Gi, N. (2015). Future changes in autumn atmospheric river events in British Columbia, Canada, as projected by CMIP5 global climate models. *Journal of Geophysical Research-Atmospheres*, *120*(18), 9279–9302. https://doi.org/10.1002/2015JD023279

Ralph, F. M., Neiman, P. J., Kiladis, G. N., Weickmann, K., & Reynolds, D. W. (2011). A multiscale observational case study of a Pacific atmospheric river exhibiting tropical–extratropical connections and a mesoscale frontal wave. *Monthly Weather Review*, *139*(4), 1169–1189. https://doi.org/10.1175/2010mwr3596.1

Ralph, F. M., Rutz, J. J., Cordeira, J. M., Dettinger, M., Anderson, M., Reynolds, D., et al. (2019). A scale to characterize the strength and impacts of atmospheric rivers. *Bulletin of the American Meteorological Society*, *100*(2), 269–290. https://doi.org/10.1175/BAMS-D-18-0023.1

Shields, C. A., & Kiehl, J. T. (2016). Atmospheric river landfall-latitude changes in future climate simulations. *Geophysical Research Letters*, *43*(16), 8775–8782. https://doi.org/10.1002/2016GL070470

Sobel, A. H., & Maloney, E. D. (2000). Effect of ENSO and the MJO on western North Pacific tropical cyclones. *Geophysical Research Letters*, *27*(12), 1739–1742. https://doi.org/10.1029/1999GL011043

Spry, C. M., Kohfeld, K. E., Allen, D. M., Dunkley, D. M., & Lertzman, K. P. (2014). Characterizing pineapple express storms in the lower mainland of British Columbia, Canada. *Canadian Water Resources Journal/Revue canadienne des ressources hydriques*, *39*(3), 302–323. https://doi.org/10.1080/07011784.2014.942574

Stan, C., Straus, D. M., Frederiksen, J. S., Lin, H., Maloney, E. D., & Schumacher, C. (2017). Review of tropical–extratropical teleconnections on intraseasonal time scales. *Reviews of Geophysics*, *55*(4), 902–937. https://doi.org/10.1002/2016RG000538

Trenberth, K. E. (1998). Atmospheric moisture residence times and cycling: Implications for rainfall rates and climate change. *Climatic Change*, *39*(4), 667–694. https://doi.org/10.1023/A:1005319109110

Waliser, D. E., & Guan, B. (2017). Extreme winds and precipitation during landfall of atmospheric rivers. *Nature Geoscience*, *10*(3), 179–183. https://doi.org/10.1038/ngeo2894

Wang, J., Kim, H., Kim, D., Henderson, S. A., Stan, C., & Maloney, E. D. (2020). MJO teleconnections over the PNA region in climate models. Part I: Performance- and process-based skill metrics. *Journal of Climate*, *33*(3), 1051–1067. https://doi.org/10.1175/JCLI-D-19-0253.1

Wang, L., & Wang, L. (2019). Impact of the East Asian winter monsoon on tropical cyclone genesis frequency over the South China Sea. *International Journal of Climatology*, *40*(2), 1328–1334. https://doi.org/10.1002/joc.6243

Warner, M. D., Mass, C. F., & Salathe, E. P. (2015). Changes in winter atmospheric rivers along the North American West Coast in CMIP5 climate models. *Journal of Hydrometeorology*, *16*(1), 118–128. https://doi.org/10.1175/JHM-D-14-0080.1

Wheeler, M. C., & Hendon, H. H. (2004). An all-season real-time multivariate MJO index: Development of an index for monitoring and prediction. *Monthly Weather Review*, *132*(8), 1917–1932. https://doi.org/10.1175/1520-0493(2004)132<1917:AARMMI>2.0.CO;2

Wolding, B. O., Maloney, E. D., Henderson, S., & Branson, M. (2017). Climate change and the Madden–Julian Oscillation: A vertically resolved weak temperature gradient analysis. *Journal of Advances in Modeling Earth Systems*, *9*(1), 307–331. https://doi.org/10.1002/2016MS000843

Xu, G., Ma, X., Chang, P., & Wang, L. (2020). A comparison of Northern Hemisphere atmospheric rivers detected by a new image-processing based method and magnitude-thresholding based methods. *Atmosphere*, *11*(6), 628. https://www.mdpi.com/2073-4433/11/6/628

Yasunaga, K., & Mapes, B. (2012). Differences between more divergent and more rotational types of convectively coupled equatorial waves. Part I: Space–time spectral analyses. *Journal of the Atmospheric Sciences*, *69*(1), 3–16. https://doi.org/10.1175/JAS-D-11-033.1

Zhang, C. D. (2005). Madden-Julian Oscillation. *Reviews of Geophysics*, *43*(2), 158–194. https://doi.org/10.1029/2004RG000158

Zhang, C. D. (2013). Madden-Julian Oscillation: Bridging weather and climate. *Bulletin of the American Meteorological Society*, *94*(12), 1849–1870. https://doi.org/10.1175/BAMS-D-12-00026.1

Zhang, Z., Ralph, F. M., & Zheng, M. (2019). The relationship between extratropical cyclone strength and atmospheric river intensity and position. *Geophysical Research Letters*, *46*(3), 1814–1823. https://doi.org/10.1029/2018GL079071

Zheng, C., Chang, E. K. M., Kim, H., Zhang, M., & Wang, W. (2018). Impacts of the Madden-Julian Oscillation on storm-track activity, surface air temperature, and precipitation over North America. *Journal of Climate*, *31*(15), 6113–6134. https://doi.org/10.1175/JCLI-D-17-0534.1

Zhou, W., Yang, D., Xie, S., & Ma, J. (2020). Amplified Madden-Julian Oscillation impacts in the Pacific–North America region. *Nature Climate Change*, *10*(7), 654–660. https://doi.org/10.1038/s41558-020-0814-0

Zhou, Y., & Kim, H. (2019). Impact of distinct origin locations on the life cycles of landfalling atmospheric rivers over the U.S. West Coast. *Journal of Geophysical Research: Atmospheres*, *124*(22), 11897–11909. https://doi.org/10.1029/2019JD031218

Zhou, Y., Kim, H., & Guan, B. (2018). Life cycle of atmospheric rivers: Identification and climatological characteristics. *Journal of Geophysical Research: Atmospheres*, *123*(22), 12715–12725. https://doi.org/10.1029/2018JD029180